Retinal stray light originating from intraocular lenses and its effect on visual performance

van der Mooren, Marie Huibert

Chapter 8

Effect of glistenings in intraocular lenses

Reprinted from Biomedical Optics Express, Vol. 8, van der Mooren M, Fransen L, Piers P Pages 1294-1304 Copyright © 2013, with permission from Optical Society of America.

AMO Groningen BV, Netherlands (van der Mooren, Franssen, Piers)

http://dx.doi.org/10.1364/BOE.4.001294

The authors acknowledge Tom van den Berg, Michelle Langeslag and Joris Coppens for their contributions to this paper. We acknowledge financial support from EUREKA grant INT 111017.

Abstract

Glistenings consist of multiple microvacuoles in intraocular lenses (IOLs) that cause retinal stray light and may affect quality of vision. For four IOL types, the microvacuole particle size distribution and particle volume density was measured using confocal light microscopy and dark field microscopy, and the corresponding extinction coefficient γ was determined. The light scatter contribution induced by microvacuoles was measured as function of both angle and extinction, and was verified by calculations using Mie theory. Two IOL types possessed significant glistenings having stray light levels higher than that of a healthy 20 year old crystalline lens corresponding to $\gamma \geq 0.08$ mm^{-1}

OCIS codes: (330.4595) Optical effects on vision; (290.2648) Stray light; (330.4460) Ophthalmic optics and devices

1 Introduction

The phenomenon of inclusions or microvacuoles in intraocular lenses (IOLs) has been discussed extensively in ophthalmic literature for more than twenty five years. They are often referred to as glistenings due to their appearance when visualized e.g. in a slit-lamp exam. In our study, we consider a microvacuole to be a void located in the IOL bulk filled with the fluid surrounding the IOL. Glistenings are considered to be the visual effect caused by multiple microvacuoles. This study describes how light propagates through a lens containing such microvacuoles and discusses the effects on quality of vision based on the light intensity distribution as a function of retinal eccentricity. Several papers report clinical studies investigating the impact of glistenings in intraocular lenses on contrast sensitivity (CS) and visual acuity (VA). In total, 6 studies examined the effect of glistenings on CS. Four of these studies reported that glistenings had a significant negative effect on the high spatial frequency CS [1–4] and two studies were non-conclusive [5,6]. While some studies do show a decrease in VA with increased severity of glistenings [6,7] the general consensus in the literature tends to be that visual acuity is unaffected by glistenings [1–3,5,8–13]. These studies found no common conclusion concerning the effect of glistenings on measured visual quality. This may be due to the fact that quality of vision is not measurable in one comprehensive test and the aforementioned standard vision testing methodologies require only a very small part of the retina to respond to stimuli. *In vitro* studies report a positively correlated relationship between the total integrated light scatter and the severity of glistenings [14,15]. Also, several *in vivo* studies found increased levels of intraocular stray light [8,13,16]. *In vitro* studies allow us to isolate the scatter contribution of the IOL from that of the ocular media. They enable the study of light scatter patterns from the patients' perspective, i.e. in the forward direction, and also from the clinicians' perspective, i.e. in the backward direction [17]. Absorption removes and scattering redirects energy from the propagating light beam forming the retinal image. The attenuation in light intensity of the original beam is called extinction and this phenomenon is described by Beer's law. The transmitted light intensity decreases exponentially with the path length traveled by the propagating beam in a medium, in our case the IOL. Microvacuoles are almost completely transparent in visible light. For the visible wavelength range, absorption plays no role in light attenuation caused by the microvacuoles, and the effects measured are solely caused by scattering. In addition to light scatter measurements, it is also possible to perform light microscopy on the same IOL. In this paper, our aim is to relate microvacuole density and size distribution to light scatter as a function of visual angle based on Mie theory. Mie formulae are applied in various scientific fields from chemistry, medicine and astronomy to meteorology. The lunar corona shown in Fig. 1 illustrates the optical effects of the clouds in front of the bright moon acting both as a grating and as a prism [18].

Fig. 1. Lunar corona.

The water droplets in a cloud separate the incident moon light into two optical fields. One field consists of the light diffracted by the surfaces of the water droplets creating a white halo and the other field traverses the water droplets creating colored fringes. The strength and size of the halo is determined by the density and size distribution of the water droplets. The lunar corona is an anomalous scattering pattern because it is composed of two optical fields. The water droplets in the cloud act similarly to the microvacuoles in the intraocular lenses. In this paper, methods used in atmospheric optics are applied for our specific investigation by adapting all parameters applicable such as refractive indices and particle distribution. This study presents measurements of light scatter and extinction determination based on confocal light microscopy and dark field microscopy for IOLs containing microvacuoles. The angular distribution of the scatter function will provide information that can be used to optimize a clinical setup to test the influence of microvacuoles on visual performance. Our findings also explain various literature reports on contrast sensitivity and visual acuity related to glistenings in clinical studies.

2. Materials and methods

The following sixteen hydrophobic acrylic IOLs were included in this study: five Acrysof IOLs (Alcon Laboratories Inc, Forth Worth, Texas, USA), three iSymm IOLs (HOYA Surgical Optics Inc, Singapore), three enVista IOLs (Bausch & Lomb, Rochester, New York, USA) and five Tecnis IOLs (Abbott Medical Optics Inc, Santa Ana, California, USA). All lenses were removed from their packages and directly immersed in saline solution in fluid cells. Microvacuoles were induced by taking the IOL from its room temperature environment and placing it into an oven at ocular temperature of 35 °C for a period of more than 8 hours. The lenses were removed from the oven for measurement at room temperature. The densities of induced microvacuoles vary with the time following their removal from the oven. For this reason, restrictions were made with respect to the time points of

measurements. The light scatter measurements and lens imaging with confocal microscopy and dark field microscopy were performed within a two-hour period. Confocal microscopy has a limited depth of focus, as such multiple images were made throughout the thickness of the lens and the images were then stacked. It also has a small field of view resulting in the need for three or more lateral displacements across the lens in order to image the complete central optic body. Dark field microscopy is a setup where the intraocular lens is retro-illuminated with an annulus of light and has a large field of view. If there are no inclusions or other sources for light scatter, the image will be black. The Image J program was used to determine size and density of the microvacuoles from the stacked confocal microscopy images for dense populations or from dark field microscopy photographs for tiny populations of microvacuoles. The size distribution and density together with the indices of refraction for microvacuole and IOL material contribute to the extinction coefficient γ [mm^{-1}], shortened to extinction in this paper. For each IOL γ was determined using Eq. (1) [19], where *N(a)* is the microvacuole size distribution per unit volume and "a" is the microvacuole radius and *Q* is the scatter extinction efficiency factor defined in Eq. (2) [19]. The phase lag ρ experienced by the central ray that passes through the full diameter of the microvacuole is $2ka|m\text{-}1|$, where *m* is the ratio of the refractive indices of microvacuole and IOL material *n*. Wave number *k* is equal to $2\pi n/\lambda$ where λ is the wavelength of light used.

$$\gamma = \int_0^\infty \pi a^2 Q(a) N(a) da \tag{1}$$

$$Q(\rho)=2-(4/\rho)\sin\rho+(4/\rho^2)(1-\cos\rho) \tag{2}$$

Factor *Q* oscillates around the value of 2 illustrating the efficiency for light scatter in large particles. The oscillation damps with increasing phase lag.

2.1. Light scatter measurements

Using two lab-based methods, the scattered light intensity distribution was measured as a function of angle. These in vitro light scatter methods capturing the high dynamic angular and intensity range have previously been described by van der Mooren et al [20]. The output of these two methods is expressed in a scatter parameter *s* [deg^2/sr] defined as point spread function *PSF(θ)* multiplied by the square of visual angle θ. In the first method used to make small angle measurements, an artificial cornea was included in order to measure physiologically realistic stray light contributions close to the focal point. The second method that measures at angles larger than three degrees is able to measure the forward and backward scatter. The measured outcomes were compared with the light scatter levels for 20 yr and 70 yr old healthy crystalline lenses.

To isolate the light scatter induced by the microvacuoles, light scatter measurements with and without microvacuole induction were subtracted from each other. These results were compared to calculations using implemented Mie theory in the MIEPlot software program [21]. The measured particle distributions were introduced in the program together with the refractive indices for the IOL materials, and n = 1.33 for the microvacuoles. The MIEplot software program outputs the angular intensity distribution I(θ) over 360 degrees with a chosen angular resolution of 0.1 degrees, and is normalized to 1 by integration over the forward hemisphere. The fraction of the incident light intensity which was scattered is defined in Eq. (3) where t is the thickness of the lens.

$$f(\gamma) = 1 - \exp(-\gamma t) \tag{3}$$

The scatter function was then calculated by multiplying this fraction by the normalized intensity distribution and the angle squared as shown in Eq. (4).

$$s(\theta,\gamma) = f(\gamma) I(\theta)\, \theta^2 \tag{4}$$

Furthermore, the calculated intensity distribution I(θ) outcome was verified with Mie theory using Eq. (5). The formula consists of the sum of a refracted part [19] with $\mu = m-1$ and $x = ka$ and the Fraunhofer diffraction pattern described by the standard Bessel function J_1.

$$I(\theta) = 4\mu^2 x^2/(4\mu^2 + \theta^2)^2 + x^4((1+\cos\theta)/2)^2 (J_1(x\sin\theta)/x\sin\theta)^2 \tag{5}$$

2.2. Simulated visual effect

A slit-lamp exam performed by a surgeon, gives information that is related to the backward scatter position, whereas the patient perceives forward scatter. For particles smaller than the wavelength of light, the scatter is uniformly distributed and the surgeon can therefore adequately assess the level of intraocular scatter. When the particle size is larger than the wavelength of visible light, forward scatter is much stronger than backward scatter. A slitlamp image at 45 degrees was taken to illustrate this effect. The ratio between the forward and backward scattered intensities for this angle was calculated by using the MIEplot program. Light transmittance through an IOL is of importance for maintaining contrast throughput. The portion of the incoming light that is scattered over the retina reduces image contrast. In this study, the light transmission through an IOL was calculated as a function of extinction. Fresnel reflections, blue and UV filters and other features affecting light transmission were excluded and only the effect of the presence of microvacuoles was assessed. For all lenses that followed the procedure for microvacuole induction, the fraction of light intensity left for image formation was

calculated as exp(-γt) and expressed as the percentage of light transmission for t = 0.5mm. Contrast was defined in terms of background luminance L_b and target luminance L_t as (L_t - L_b) / L_b. For a uniform background, the luminance contrast agrees well with perceived contrast. The luminance L_v [cd/m2], which is added as retinal veiling glare to an image, is predicted by sE/θ^2, where E is the illuminance [lux] at the eye from a glare source at an angle θ. This concept of equivalent veiling luminance was introduced by Stiles and Holladay [22] for steady-state conditions. They found for a broad field of view (1 to 30 degrees) a constant value of s = 10 for phakic subjects. In our study, for pseudophakia, s was approximated with $s(\theta,\gamma)$ for the microvacuole effect and a constant value of 10 was added based on the average stray light level of various IOLs obtained by 220 stray light measurements with an extended glare source [23]. The effect of glare is demonstrated by the luminance contrast described in Eq. (6).

$$C = (L_t - L_b) / (L_b - L_v) \quad (6)$$

The perceived contrast varies across the image not only because of the angular scatter function but also because it is dependent on the condition and task the subject is performing. As illustrative examples, we calculated the impact on contrast vision as a function of extinction for three tasks with the different lighting conditions defined in Table 1.

Table 1 Description of three daily tasks under different conditions

condition	L_t [cd/m^2]	E[lux]	θ[deg]	L_b [cd/m^2]
1. Night driving with oncoming car	1	0.34	3	0.5
2. Computer screen next to window	200	150	7	20
3. Contrast sensitivity test with glare	85	10	7	2

L_t is the luminance of the object to discern and L_b is the background luminance with a glare source with illuminance E at angular distance θ.

The first set of lighting conditions describes a night driving situation where the background road luminance was set to 0.5 cd/m^2. An oncoming car at a distance of 100 meters at an angle of 3 degrees has a headlight illuminance of 0.34 lux at the eye of the driver. The condition for veiling glare was considered constant for some period of time because when the oncoming car comes closer the ratio E/θ^2 is constant. The illuminance increases quadratic with distance and the ratio is kept constant due to the increase in angle. The driver had to discern a crossing pedestrian with a luminance of 1 cd/m^2. The second set of lighting conditions describes an office where an employee works behind a computer screen with luminance variation from 200 cd/m^2 to 20 cd/m^2 next to a window illuminating 150 lux of daylight at the employee's eye. The third set of lighting conditions describes that of a dark clinical measurement lane where a subject performs a contrast sensitivity test (L_t = 85 cd/m^2, L_b = 2 cd/m^2) with a glare source.

3. Results

An overview of the lenses tested is given in Fig. 2 together with their measured microvacuole characteristics.

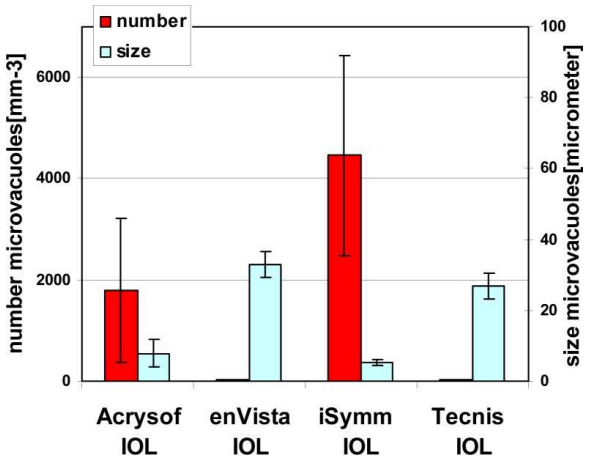

Fig. 2. Microvacuole characteristics. The error bars indicate the standard deviation. The numbers of microvacuoles per cubic millimeter for the enVista IOLs and the Tecnis IOLs are so small that the bars are hardly visible.

The lenses were tested on one of the two available stray light methods due to time constraints of the methodology. The top row of Fig. 3 displays dark field images that correspond to the confocal microscopy images shown in the bottom row for all four types of IOLs.

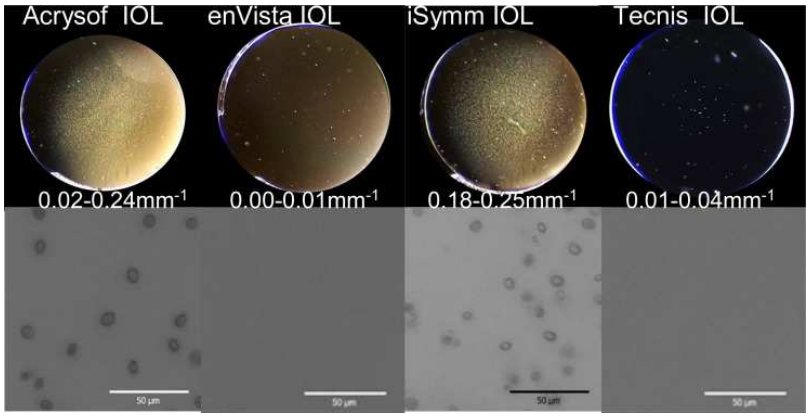

Fig. 3. Top row shows dark field images and bottom row confocal images. The range of the extinction coefficients is displayed in between rows. The images from left to right with γ = 0.11mm^{-1}, γ = 0.00 mm^{-1}, γ = 0.18 mm^{-1} and γ = 0.02 mm^{-1}. Bar indicates 50 µm.

The microvacuoles are non-spherical and an effective diameter is used to characterize the size while the non-uniformity of sizes is characterized by the standard deviation. For the Acrysof lenses the number of microvacuoles ranged from 46 to 3862 per cubic mm. The number of microvacuoles for the iSymm IOLs ranged from 2545 to 6495 per cubic mm, for the enVista IOLs 3 to 6 microvacuoles per cubic mm were found and the number for the Tecnis lenses ranged from 12 to 36 microvacuoles per cubic mm. The microvacuoles in the enVista IOLs had an effective diameter of approximately 33 µm and in the Tecnis IOLs 25 µm while the sizes in the iSymm IOLs and Acrysof IOLs were significantly smaller, 5.2 µm and 6.2 µm, respectively. For all cases, the standard deviation is approximately 30% of the average microvacuole diameter. The phase lag ρ was larger than 5 for all cases, and the scatter efficiency factor Q was equal to 2 for all lenses. This means that for all lenses the refracted scatter is incoherent, and that twice the intensity incident on a microvacuole was scattered. The extinction was calculated according to Eq. (1) for all IOLs and ranged from 0.02 to 0.24 mm^{-1} for Acrysof lenses. For the enVista IOLs γ ranged from 0.00 to 0.01 mm^{-1}, for the iSymm IOLs γ ranged from 0.18 to 0.25 mm^{-1}, and for the Tecnis lenses γ ranged from 0.01 to 0.04 mm^{-1}.

3.1. Light scatter measurements

Figure 4 displays all light scatter measurement results after microvacuole induction and are labeled with the corresponding measured extinctions that can be found in the legend. The scatter measurements at three degrees showed a higher than expected outcome because of the large angular width (1.2 degrees) of the camera aperture [20] relative to the measurement angle. In that study [20] the measurement result performed on one lens without any glistenings on both setups agreed well. In Fig. 4 the measurement results of both methods are displayed for different lenses with different levels of glistenings, and the results of both methods agree well with theory as shown in Fig. 5 and will be described later. For the lenses which have low extinctions the results between the two methods deviate due to very low signal levels, but are well below the level of a 20 yr old crystalline lens. In general, it is found that when γ is smaller than 0.08 mm^{-1}, the light scatter is less than that of a 20 yr old crystalline lens, and when γ is larger than approximately 0.25 mm^{-1}, the light scatter is more than that of a 70 yr old crystalline lens. For extinctions between 0.08 mm^{-1} and 0.25 mm^{-1}, the light scatter level is between that of a 20 yr old and 70 yr old crystalline lens. Two scatter functions $s(\theta, \gamma = 0.11)$ and $s(\theta, \gamma = 0.24)$ calculated using MIEplot for microvacuoles with an average diameter of 6 µm and a standard deviation of 2 µm are displayed in Fig. 5. The stray light function shows two peaks, one at two degrees and a broader peak at 15 degrees. These calculations compare well to the optical scatter levels induced, obtained from the subtraction of measurements results after and before microvacuole induction.

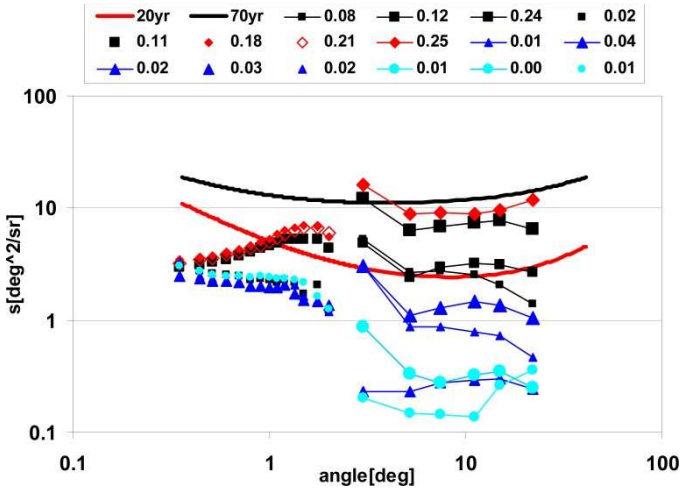

Fig. 4. Scatter level as a function of visual angle compared to a 20 yr and a 70 yr old healthy crystalline lens. The numbers in the legend denote extinction and symbols in the graph denote the IOL type ***(▪Acrysof, ●enVista, ◊ and ♦iSymm, ΔTecnis).*** *The low angle measurements are represented with symbols; the actual measurements have much higher resolution.*

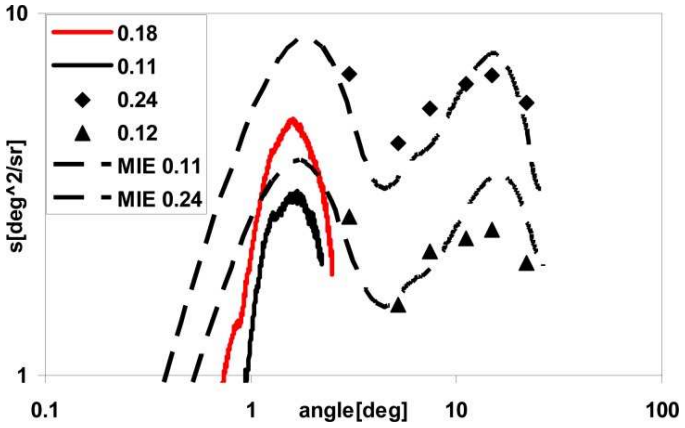

Fig. 5. Induced light scatter of two small-angle (solid black line γ = 0.11 mm^{-1} and solid redline γ = 0.18 mm^{-1}) and two large-angle measurements (symbols: γ = 0.12 mm^{-1} and γ = 0.24 mm^{-1}) compared to two outcomes using MIEPlot program for γ = 0.11 and 0.24 mm^{-1} (dashed).

The lower scatter angle measurements show lower peaks and narrower widths than the calculations. It is important to take note of the fact that the results are displayed on a log-log scale and the difference in width is within 1 degree, and the peak difference is approximately 1 deg^2/sr. The measured red curve had an extinction of 0.18 mm^{-1}, and the

peak is as expected in between the calculated values of 0.11 mm^{-1} and 0.24 mm^{-1}. The decomposed scatter intensity outcomes of the MIEplot program compare well with MIE-theory formulated in Eq. (5). The peak at two degrees is caused by diffraction and the peak at 15 degrees by refraction of light traversing the microvacuoles.

3.2. Simulated visual effect

In Fig. 6, an Acrysof IOL is shown viewed with slit illumination at 45 degrees in the forward and backward direction, and both images were scaled to the same intensity level. The calculated intensity ratio between forward and backward scatter for this angle is 390. For all lenses with microvacuoles, light intensity transmission is calculated using Beer's law shown in Fig. 7. The enVista IOL transmitted 100%, the four Tecnis IOLs at least 98%, the two iSymm IOLs transmitted approximately 90%, and the Acrysof IOLs show a variable performance level between 89% and 99%. This can be seen as the percentage of light remaining for image formation.

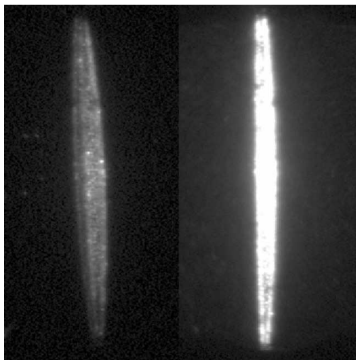

Fig. 6. Backward (left) and Forward (right) scatter for Acrysof lens at 45 degrees [17].

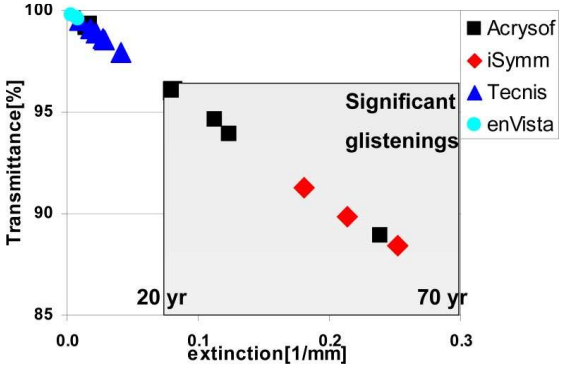

Fig. 7. Light transmission (%) left for image formation.

The results of the luminance contrast calculations are shown in Fig. 8 for each set of lighting conditions presented in Table 1. In each case, the contrast decreases with increasing level of extinction. For an extinction of 0.15 mm^{-1}, the contrast dropped 19%, 17% and 15% respectively for case 1, 2 and 3 compared to an IOL with no microvacuoles. For case 3, the background luminance is very small compared to the target luminance and the contrast is determined by L_t/L_v. In this case, the contrast reduction can be determined directly from the light intensity transmission graph (Fig. 7). When γ = 0.15 mm^{-1}, the intensity transmittance for image formation is 92.5%. Correspondingly, the light scattered is 7.5%, which is half of the percentage of the contrast reduction.

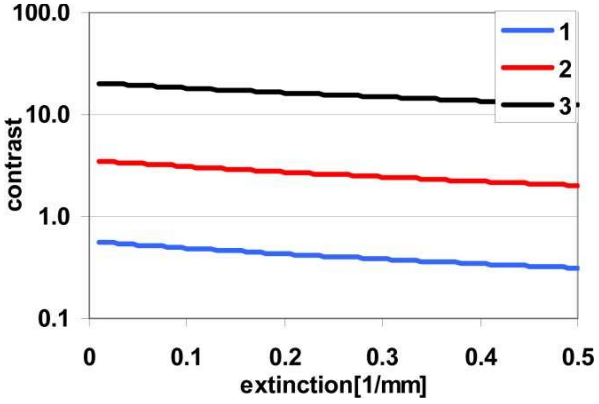

Fig. 8. Luminance contrast as a function of extinction for three common daily tasks. Labels refer to the lighting conditions defined in Table 1.

4. Discussion

Several recent studies, based on large numbers of patients implanted with Acrysof IOLs (≈100 patients or more) conclude that moderate to severe/dense glistenings occur in 60-87% of patients implanted with these lenses [4,5,9,13,24]. The glistenings formation, as well as the severity of glistenings, has been correlated with longer follow-up times [3,7,10,24–26]. Very few studies that evaluate the progression beyond one year find glistening formation to be stable [5,6]. Temperature fluctuations in the eye are mentioned as one of the factors for this progression. *In vitro* we also observed an increase in glistening formation when cyclical temperature changes were induced. The extinction values for two Acrysof IOLs progressed from 0.08 mm^{-1} and 0.12 mm^{-1} to 0.29 mm^{-1} when the procedure for microvacuole induction was repeated two times. Following cyclical temperature changes induced stray light values above that of the healthy 70 year old crystalline lens. The Tecnis IOLs made of the acrylic Sensar material were not associated with glistenings except for only one *in vitro* study that found minimal non-significant glistenings [27]. The enVista IOLs claim to be glistenings-free. The qualifications, non-significant glistenings and glistenings-free are arbitrary and our study enables us to define and grade glistenings in a functional and quantitative way. We define a lens with significant glistenings to be a lens that has microvacuoles such that it causes stray light levels to be raised above those of a healthy 20 year old crystalline lens. This level of stray light is further specified as $\gamma \geq 0.08\ mm^{-1}$, which corresponds to 4% light scatter of the incident light beam. According to this definition, all three iSymm IOLs and four of the five Acrysof IOLs were associated with significant glistenings (Fig. 7) and correspondingly with a light transmittance that is less than 96%. Although, no studies have been published in English language literature, for the iSymm IOLs, our *in vitro* method of microvacuole formation shows similar trends to what is found in published *in vivo* studies. We acknowledge that our investigational technique is not necessarily an exact simulation of how all investigated IOLs will respond *in vivo*. Microvacuole induction in IOLs is a dynamic process and the applied time constraints for measurements were necessary to investigate the relationship between the determined extinctions and measured light scatter levels. A controlled waiting period was used directly after the lens had been removed from the oven (eye temperature) to allow for the condensation formation to disappear. During induction, it was observed that the microvacuoles originate from the center of the lens and spread out towards the periphery of the lens optic. When the lens is in a constant temperature environment for more than a day, all microvacuoles disappear. The material close to the edges and lens surfaces is free from the microvacuoles that are denser close to the visual axis (Fig. 9).

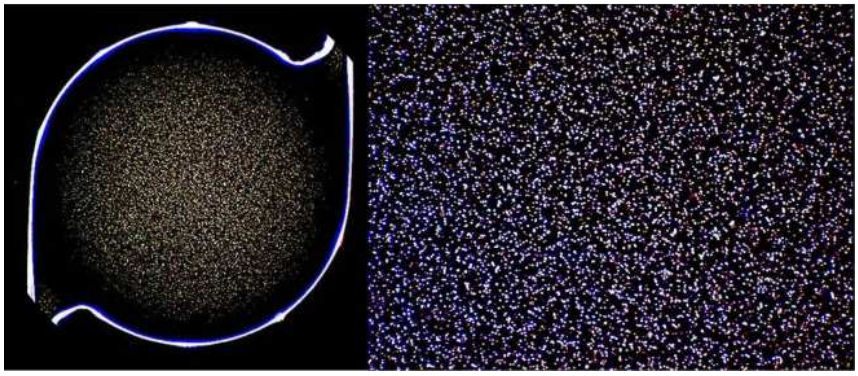

Fig. 9. Dark field images Acrysof lens 10X (left) and 40X (right).

Microvacuoles are thought to be caused by a combination of material and manufacturing process related factors. Reports from Japan discuss surface light scatter and nano-glistenings present at the surface of the Acrysof IOL [28–33]. This surface phenomenon is not incorporated in the analysis performed in the present study. We focused on the glistenings in the bulk of the IOL and their impact on vision. Additional stray light and dark field microscopy measurements were performed on five Acrysof lenses intended for the Japanese market. For these lenses it was claimed that glistenings were reduced following improvements in the manufacturing process. These IOLs had stray light values of approximately 7 deg^2/sr at two degrees, results that are typical for extinction values between 0.11 mm^{-1} and 0.18 mm^{-1} such as are shown in Fig. 3. Dark field microscopy images for two magnifications are shown in Fig. 9 for one lens. The determination of the extinction of an IOL with microvacuoles elucidates the basic principles of the scatter process. The calculated scatter efficiency factor of two in all cases measured in this study supports the idea of the existence of two optical fields. From the measurements performed, it can be concluded that the extinction of an IOL or light attenuation from an incident beam can be compared with the age-related increase in light scatter found in the natural crystalline lens. The induced light scatter measured in the presence of the microvacuoles show two peaks determined by diffraction and refraction that are verified by Mie theory and resemble the effect of a lunar corona, i.e. a white halo and a colored band. The surgeon may underestimate the significance of the phenomenon of glistenings in an IOL slit-lamp exam because the forward scatter perceived by the patient is more than 300 fold stronger than the observed backward scatter. Glare conditions are very commonly present while executing daily tasks. Common traffic scenes involve more field of view than the standard clinical vision tests. An important aspect in quality of vision is the ability to navigate in traffic whether as a pedestrian or as a vehicle driver or cyclist. Ultimately, knowing how the incident light of a scene is focused and scattered by the cornea and lens onto the retina provides information necessary to estimate the effect of

any perturbation on vision. Currently, no single clinical or pre-clinical assessment provides this information in one measurement because the light intensity used for an arbitrary daily task varies approximately nine orders of magnitude over the total retina. In this study, we made use of two *in vitro* stray light methods to obtain this information. We have shown that for three common lighting conditions, glistenings reduce contrast. When a high-contrast task is performed, the reduction caused by glistenings may not be a noticeable hindrance, while for a low-contrast task the contrast loss will have a much larger impact. To quantify the visual effect of glistenings, we can simulate from the induced light transmission loss the contrast reduction for tasks where the background luminance is low compared to target luminance.

Most clinical studies report that glistenings have no effect on visual acuity. This can be explained by the induced scatter function obtained as a function of visual angle as shown in Fig. 5. A visual acuity of 20/20 corresponds to less than 0.02 degrees of visual angle. For the small angles used in VA measurements, scatter plays a less significant role than for larger angles. This changes when target luminance and target contrast are low causing reduced retinal image contrast due to the lower light transmission for image formation. This conclusion is supported by studies that show a decrease in contrast sensitivity especially for higher spatial frequencies. For the higher spatial frequencies, the contrast sensitivity is lowest. Standard contrast vision tests have steps between consecutive levels of 40%. Not all studies find an effect for all spatial frequencies because in order to consistently illustrate the effect of stray light for these viewing conditions, extinction levels of at least 0.20 $mm^{-1}$are necessary. To consistently measure the clinical effect of glistenings on vision, contrast steps smaller than 40% should be used. Additionally, low-contrast examinations with low luminance, or contrast tests where the glare source is positioned at angles close to that of the scatter function maxima, could also illustrate the effect of glistenings.

In summary, the size, distribution, and density, together with the indices of refraction for microvacuoles and IOL materials contribute to the extinction coefficient *γ.* We have shown that glistenings can be quantified in this one parameter, the extinction coefficient, and that their impact on contrast vision can be simulated using the veiling luminance. The iSymm IOLs and the majority of the Acrysof IOLs showed significant levels of glistenings. It can be concluded that IOL manufacturers should consider evaluating IOL stray light as a standard procedure in the release of new IOL models. In addition, it can be concluded that in order to ensure that glistenings do not cause a significant increase in stray light, the extinction coefficient should remain below 0.08 mm^{-1}, that which results in a stray light level equivalent to a 20 yr old healthy crystalline lens.

References en links

1. D. K. Dhaliwal, N. Mamalis, R. J. Olson, A. S. Crandall, P. Zimmerman, O. C. Alldredge, F. J. Durcan, and O. Omar, "Visual significance of glistenings seen in the AcrySof intraocular lens," J. Cataract Refract. Surg. **22**(4), 452–457 (1996).
2. U. Gunenc, F. H. Oner, S. Tongal, and M. Ferliel, "Effects on visual function of glistenings and folding marks in AcrySof intraocular lenses," J. Cataract Refract. Surg. **27**(10), 1611–1614 (2001).
3. A. Waite, N. Faulkner, and R. J. Olson, "Glistenings in the single-piece, hydrophobic, acrylic intraocular lenses," Am. J. Ophthalmol. **144**(1), 143–144 (2007).
4. H. Minami, K. Toru, K. Hiroi, and S. Kazama, "Glistening of Acrylic Intraocular Lenses," Rinsho Ganka **53**(5), 991–994 (1999) (Jpn. J. Clin. Ophthalmol.).
5. J. Colin and I. Orignac, "Glistenings on intraocular lenses in healthy eyes: effects and associations," J. Refract. Surg. **27**(12), 869–875 (2011).
6. G. Christiansen, F. J. Durcan, R. J. Olson, and K. Christiansen, "Glistenings in the AcrySof intraocular lens: pilot study," J. Cataract Refract. Surg. **27**(5), 728–733 (2001).
7. J. Colin, D. Praud, D. Touboul, and C. Schweitzer, "Incidence of glistenings with the latest generation of yellowtinted hydrophobic acrylic intraocular lenses," J. Cataract Refract. Surg. **38**(7), 1140–1146 (2012).
8. K. Hayashi, A. Hirata, M. Yoshida, K. Yoshimura, and H. Hayashi, "Long-term effect of surface light scattering and glistenings of intraocular lenses on visual function," Am. J. Ophthalmol. **154**(2), 240–251, e2 (2012).
9. J. Colin, I. Orignac, and D. Touboul, "Glistenings in a large series of hydrophobic acrylic intraocular lenses," J. Cataract Refract. Surg. **35**(12), 2121–2126 (2009).
10. J. Moreno-Montañés, A. Alvarez, R. Rodríguez-Conde, and A. Fernández-Hortelano, "Clinical factors related to the frequency and intensity of glistenings in AcrySof intraocular lenses," J. Cataract Refract. Surg. **29**(10), 1980–1984 (2003).
11. E. Wilkins and R. J. Olson, "Glistenings with long-term follow-up of the Surgidev B20/20 polymethylmethacrylate intraocular lens," Am. J. Ophthalmol. **132**(5), 783–785 (2001).
12. L. Werner, "Glistenings and surface light scattering in intraocular lenses," J. Cataract Refract. Surg. **36**(8), 1398–1420 (2010).
13. E. Mönestam and A. Behndig, "Impact on visual function from light scattering and glistenings in intraocular lenses, a long-term study," Acta Ophthalmol. (Copenh.) **89**(8), 724–728 (2011).
14. D. H. Kim, R. H. James, R. J. Landry, D. Calogero, J. Anderson, and I. K. Ilev, "Quantification of glistenings in intraocular lenses using a ballistic-photon removing integrating-sphere method," Appl. Opt. **50**(35), 6461–6467 (2011).
15. T. Oshika, Y. Shiokawa, S. Amano, and K. Mitomo, "Influence of glistenings on the optical quality of acrylic foldable intraocular lens," Br. J. Ophthalmol. **85**(9), 1034–1037 (2001).
16. M. Nagata, H. Matsushima, K. Mukai, W. Terauchi, T. Senoo, H. Wada, and S. Yoshida, "Clinical evaluation of the transparency of hydrophobic acrylic intraocular lens optics," J. Cataract Refract. Surg. **36**(12), 2056–2060 (2010).
17. M. van der Mooren, J. Coppens, M. Bandhauer, and T. van den Berg, "Light scatter characteristics of acrylic intraocular lenses," Invest. Ophthalmol. Vis. Sci. **48**, E-abstract 3126 (2007).
18. L. Cowley, P. Laven, and M. Vollmer, "Rings around the sun and moon: coronae and diffraction," Phys. Educ. **40**(1), 51–59 (2005).
19. H.C. van de Hulst, *Light Scattering by Small Particles* (Dover Publications Inc., 1981), pp. 129, 176, 222.

20. M. van der Mooren, T. van den Berg, J. Coppens, and P. Piers, "Combining in vitro test methods for measuring light scatter in intraocular lenses," Biomed. Opt. Express **2**(3), 505–510 (2011).
21. P. Laven, "MiePlot: A computer program for scattering of light from a sphere using Mie theory & the Debye series," http://www.philiplaven.com/mieplot.htm, accessed January 2013.
22. L. L. Holladay, "The fundamentals of glare and visibility," J. Opt. Soc. Am. **12**(4), 271–319 (1926).
23. T. J. Van Den Berg, L. J. Van Rijn, R. Michael, C. Heine, T. Coeckelbergh, C. Nischler, H. Wilhelm, G. Grabner, M. Emesz, R. I. Barraquer, J. E. Coppens, and L. Franssen, "Straylight effects with aging and lens extraction," Am. J. Ophthalmol. **144**(3), 358–363, 363.e1 (2007).
24. E. Peetermans and R. Hennekes, "Long-term results of wagon wheel packed acrylic intraocular lenses (AcrySof)," Bull. Soc. Belge Ophtalmol. **271**, 45–48 (1999).
25. D. Tognetto, L. Toto, G. Sanguinetti, and G. Ravalico, "Glistenings in foldable intraocular lenses," J. Cataract Refract. Surg. **28**(7), 1211–1216 (2002).
26. S. Yoshida, H. Matsushima, M. Nagata, T. Senoo, I. Ota, and K. Miyake, "Decreased visual function due to highlevel light scattering in a hydrophobic acrylic intraocular lens," Jpn. J. Ophthalmol. **55**(1), 62–66 (2011).
27. N. Z. Gregori, T. S. Spencer, N. Mamalis, and R. J. Olson, "In vitro comparison of glistening formation among hydrophobic acrylic intraocular lenses," J. Cataract Refract. Surg. **28**(7), 1262–1268 (2002).
28. H. Nishihara, S. Yaguchi, T. Onishi, M. Chida, and M. Ayaki, "Surface scattering in implanted hydrophobic intraocular lenses," J. Cataract Refract. Surg. **29**(7), 1385–1388 (2003).
29. H. Nishihara, M. Ayaki, T. Watanabe, T. Ohnishi, T. Kageyama, and S. Yaguchi, "Comparison of surface light scattering of acrylic intraocular lenses made by lathe-cutting and cast-molding methods—long-term observation and experimental study," Nippon Ganka Gakkai Zasshi **108**(3), 157–161 (2004) (article in Japanese).
30. S. Yaguchi, H. Nishihara, W. Kambhiranond, D. Stanley, and D. J. Apple, "Light scatter on the surface of AcrySof intraocular lenses: part I. Analysis of lenses retrieved from pseudophakic postmortem human eyes," Ophthalmic Surg. Lasers Imaging **39**(3), 209–213 (2008).
31. K. Miyata, S. Otani, R. Nejima, T. Miyai, T. Samejima, M. Honbo, K. Minami, and S. Amano, "Comparison of postoperative surface light scattering of different intraocular lenses," Br. J. Ophthalmol. **93**(5), 684–687 (2009).
32. H. Matsushima, K. Mukai, M. Nagata, N. Gotoh, E. Matsui, and T. Senoo, "Analysis of surface whitening of extracted hydrophobic acrylic intraocular lenses," J. Cataract Refract. Surg. **35**(11), 1927–1934 (2009).
33. K. Miyata, M. Honbo, S. Otani, R. Nejima, and K. Minami, "Effect on visual acuity of increased surface light scattering in intraocular lenses," J. Cataract Refract. Surg. **38**(2), 221–226 (2012).